



# Very Large and Long-lasting Anisotropies Caused by Sunward Streaming Energetic Ions: Solar Orbiter and STEREO A Observations

Wenwen Wei<sup>1</sup> , Christina O. Lee<sup>1</sup> , N. Dresing<sup>2</sup> , L. Y. Khoo<sup>3</sup> , L. K. Jian<sup>4</sup> , J. G. Luhmann<sup>1</sup> , C. M. S. Cohen<sup>5</sup> , F. Fraschetti<sup>6</sup> , B. Zhuang<sup>7</sup> , J. Huang<sup>1</sup> , C. J. Owen<sup>8</sup> , G. Nicolaou<sup>8</sup> , L. Rodríguez-García<sup>9</sup> , E. Palmerio<sup>10</sup> , I. C. Jebaraj<sup>2</sup> , B. J. Lynch<sup>1,11</sup> , and F. Carcaboso<sup>4</sup>

<sup>1</sup> Space Sciences Laboratory, University of California, Berkeley, CA 94720, USA; [wwwwei@berkeley.edu](mailto:wwwwei@berkeley.edu)

<sup>2</sup> Department of Physics and Astronomy, University of Turku, FI-20014 Turku, Finland

<sup>3</sup> Department of Astrophysical Sciences, Princeton University, Princeton, NJ 08544, USA

<sup>4</sup> Heliophysics Science Division, NASA Goddard Space Flight Center, Greenbelt, MD 20771, USA

<sup>5</sup> California Institute of Technology, Pasadena, CA 91125, USA

<sup>6</sup> Center for Astrophysics, Harvard & Smithsonian, Cambridge, MA 02138, USA

<sup>7</sup> Institute for the Study of Earth, Ocean, and Space, University of New Hampshire, Durham, NH 03824, USA

<sup>8</sup> Mullard Space Science Laboratory, University College London, Holmbury St Mary, Dorking, Surrey RH5 6NT, UK

<sup>9</sup> European Space Agency (ESA), European Space Astronomy Centre (ESAC), E-28692 Villanueva de la Cañada, Madrid, Spain

<sup>10</sup> Predictive Science Inc., San Diego, CA 92121, USA

<sup>11</sup> Department of Earth, Planetary, and Space Sciences, University of California, Los Angeles, CA 90095, USA

Received 2024 July 29; revised 2024 September 2; accepted 2024 September 10; published 2024 September 27

## Abstract

The anisotropy of energetic particles provides essential information to help resolve the underlying fundamental physics of their spatial distributions, injection, acceleration, and transport processes. In this work, we report an energetic ion enhancement that is characterized by very large and long-lasting anisotropies observed by STEREO A and Solar Orbiter, which are nearly aligned along the same nominal Parker spiral. This ion enhancement appears at the rising phase of a widespread solar energetic particle event that was associated with the farside coronal mass ejection on 2022 February 15. According to our analysis, the long-lasting anisotropy resulted from the continuous injection of energetic ions from a well-connected particle source located beyond the STEREO A's orbit. Solar Orbiter also observed an interval of very large anisotropy dominated exclusively by sunward streaming ions but with the additional implication that it detected the very early phase of ion injections onto magnetic field lines that newly connected to the particle source, which is likely the first reported event of this kind. These results further illustrate how energetic particle anisotropy information, in particular from multiple observer locations, can be used to disentangle the sources and transport processes of energetic ions, even when their heliospheric context is not simple.

*Unified Astronomy Thesaurus concepts:* [Solar energetic particles \(1491\)](#); [Interplanetary magnetic fields \(824\)](#); [Solar coronal mass ejections \(310\)](#)

## 1. Introduction

Anisotropies observed in energetic particles are commonly utilized to gather insights into the spatial distributions, injection, acceleration, and transport processes of energetic particles (e.g., J. W. Bieber et al. 2002; L. C. Tan et al. 2007; N. Dresing et al. 2014; D. Lario et al. 2022; B. Zhuang et al. 2022; I. C. Jebaraj et al. 2023a). In general, anisotropy analysis can provide essential information on the spatial distributions of energetic particles, as well as on the surrounding heliospheric conditions. For single-spacecraft measurements, the compositional or energy spectral features of energetic particles can only reveal a single-point analysis in space, but anisotropy analysis could shed light on two- or three- dimensional distributions of energetic particles (L. C. Tan et al. 2007, 2012). Moreover, anisotropy is capable of indicating the particle injections from the source. For example, N. Dresing et al. (2016) utilized multispacecraft observations to identify a very anisotropic bidirectional distribution of near-relativistic electrons, which was likely formed by the solar energetic particle (SEP)

injections onto both loop legs of a magnetic cloud. Furthermore, the anisotropy characteristics are particularly valuable for distinguishing signatures of particle acceleration (I. C. Jebaraj et al. 2023b). Usually, a long-lasting anisotropy not only suggests a continuous injection of particles but also indicates ongoing acceleration of particles (J. W. Bieber et al. 2002; N. Dresing et al. 2018; W. Wei et al. 2022). Additionally, the anisotropy directly reflects the particle transport in the local environment. For example, large anisotropy values imply weak pitch angle scattering, whereas small values may relate to strong pitch angle scattering, perpendicular cross-field diffusion, or multiple mirroring in stream interaction regions (SIRs; J. R. Dwyer et al. 1997; L. C. Tan et al. 2007; Y. Wang et al. 2012; R. D. T. Strauss et al. 2017; W. Wei et al. 2019, 2022).

On 2022 February 15, a large solar eruption around 21:50 UT led to a fast coronal mass ejection (CME) and a widespread SEP event, which was observed by several spacecraft including Parker Solar Probe, Solar Orbiter, BepiColombo, Solar Terrestrial Relations Observatory (STEREO) A, Advanced Composition Explorer (ACE), and Mars Atmosphere and Volatile Evolution (MAVEN). As suggested by several recent studies (M. Mierla et al. 2022; J. Giacalone et al. 2023; C. M. S. Cohen et al. 2024; L. Y. Khoo et al. 2024; E. Palmerio et al. 2024), this CME propagated toward the Parker Solar Probe and



Original content from this work may be used under the terms of the [Creative Commons Attribution 4.0 licence](#). Any further distribution of this work must maintain attribution to the author(s) and the title of the work, journal citation and DOI.

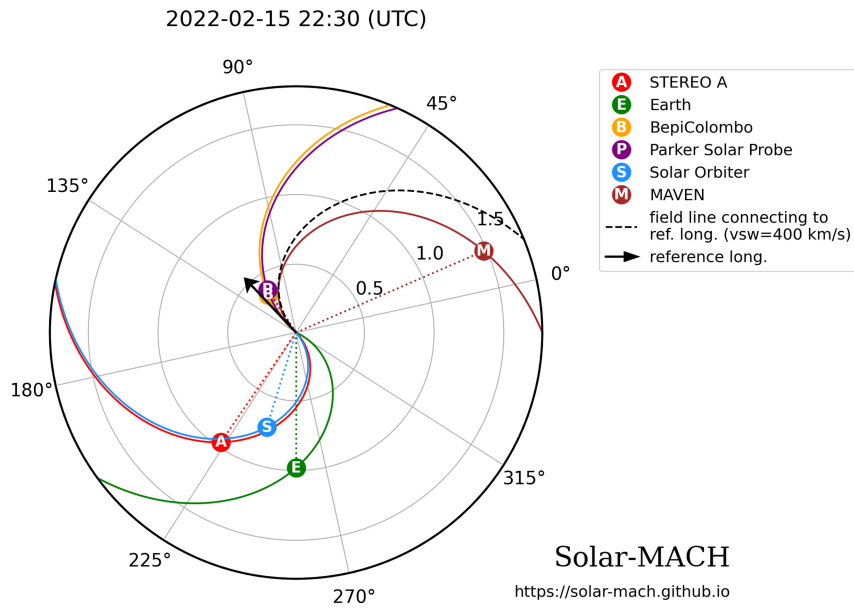


**Figure 1.** Positions of Solar Orbiter and STEREO A along with other spacecraft and planets in the inner solar system during the 2022 February 15 CME event, which was created using the Solar-MACH tool (J. Gieseler et al. 2023). The CME propagation direction is marked by the black arrow, and the positions of several spacecraft and planets are indicated by the colored symbols, as listed in the legend. Solid curves indicate the nominal Parker spiral lines connecting the Sun to different spacecraft, based on their observed solar wind speeds at 2022 February 15 22:30:00 UTC, with Solar Orbiter recording a solar wind speed of  $310 \text{ km s}^{-1}$  and STEREO A recording  $303 \text{ km s}^{-1}$ .

BepiColombo, as shown in Figure 1, whereas it was recognized as a farside event for Solar Orbiter, STEREO A, and near-Earth observers, providing an excellent opportunity to study the radial and longitudinal evolution of SEPs from the farside. Specifically, during the rising phase of the widespread SEP event observed by Solar Orbiter and STEREO A, an energetic ion enhancement characterized by very large anisotropy that lasted for about 11 hr was observed, making this event of special interest toward disentangling the spatial distributions, injection, acceleration, and transport of energetic particles.

In this work, we focus on this event to analyze the origins of its uncommon anisotropy features based on the observations from Solar Orbiter and STEREO A that cover different radial and longitudinal distances while being nearly aligned along the same nominal Parker spiral, as indicated by Figure 1. In Section 2, we introduce the data used in this work. The observations and discussion of this event are presented in Sections 3 and 4, respectively. Finally, Section 5 summarizes our main results.

## 2. Data

The STEREO A and B spacecraft (M. L. Kaiser et al. 2008) were launched in 2006, and both spacecraft orbit around the Sun near 1 au. The Plasma and Suprathermal Ion Composition (PLASTIC; A. B. Galvin et al. 2008) experiment and the In-situ Measurements of Particles and CME Transients (IMPACT; J. G. Luhmann et al. 2008) suite provide the data used in this work. The solar wind plasma parameters are measured by PLASTIC. The Magnetic Field Experiment (MAG; M. H. Acuña et al. 2008) instrument and the Solar Wind Electron Analyzer (SWEA; J. A. Sauvaud et al. 2008) onboard IMPACT give the magnetic field data and the suprathermal electron pitch angle distributions (e-PADs), respectively. The above data cadence used in this work is 1 minute. The energetic particles, including electrons, protons, and heavy ions, are detected by several

different sensors of the IMPACT suite. The Solar Electron and Proton Telescope (SEPT; R. Müller-Mellin et al. 2008) measures ions from 70 to  $7000 \text{ keV nuc}^{-1}$ . Because SEPT cannot resolve the elemental species, all ions contribute to the ion channels. In this study, we note that the protons contribute predominantly to the SEPT measurements during this event. The time resolution of the energetic ions data is downsampled to 10 minutes from the native resolution of 1 minute. In addition, SEPT was designed to give anisotropy information in four different viewing directions, with “Sun” and “Asun” originally pointing sunward and antisunward along the nominal Parker spiral, respectively, and “North” and “South” directing toward the north and south ecliptic poles, respectively. However, the spacecraft rolled by  $180^\circ$  about the spacecraft–Sun line in 2015 July to maintain Earth communications after its solar conjunction, so these nominal pointing directions changed, with the “Sun” and “Asun” telescopes pointing perpendicular to the nominal Parker spiral direction, with “North” pointing southward and “South” pointing northward (N. Dresing et al. 2023).

The Solar Orbiter mission (D. Müller et al. 2020) was launched on 2020 February 10. The magnetic field measurements are obtained by the magnetometer (MAG; T. S. Horbury et al. 2020), and the magnetic field data used in this work have a time cadence of 1 minute. The Solar Wind Plasma Analyser (SWA; C. J. Owen et al. 2020) provides the in situ solar wind measurements, and the cadence is 4 s. The Energetic Particle Detector (EPD; J. Rodríguez-Pacheco et al. 2020) is an instrument suite that measures energetic particles from a few  $\text{keV nuc}^{-1}$  to hundreds of  $\text{MeV nuc}^{-1}$ . In this work, we mainly use the energetic ions data detected by the Electron Proton Telescope (EPT), and the time resolution of the energetic ions data is averaged down from 1 s to 10 minutes. The EPT telescope also has four viewing directions, with “Sun” and “Asun” pointing sunward and antisunward along the nominal Parker spiral, respectively, and “North” and “South” directing

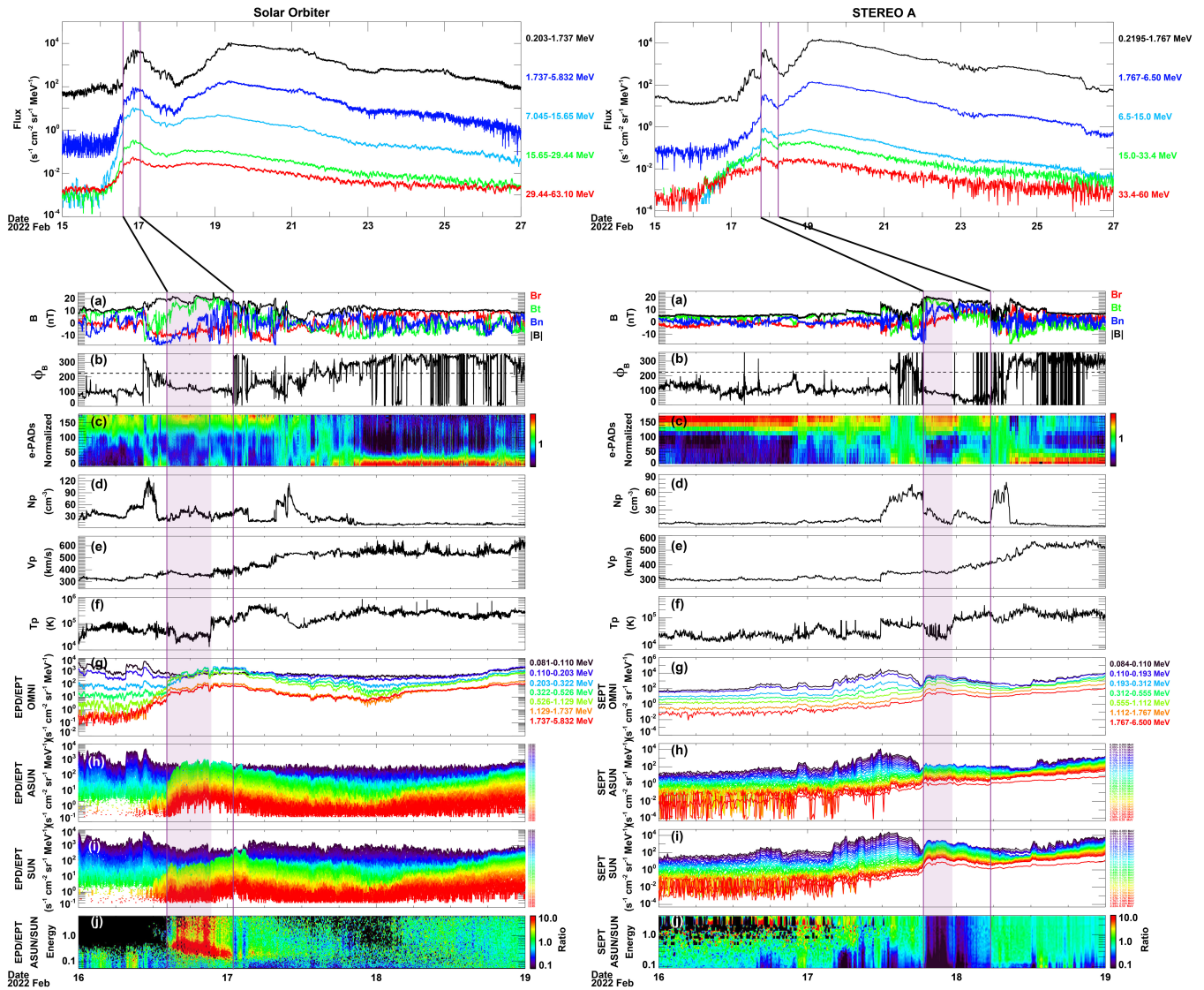


**Figure 2.** Overview of Solar Orbiter (left figure) and STEREO A (right figure) observations during 2022 February 16–19. For each of the figures, the top panel exhibits the energetic ion intensities of the widespread SEP event at several selected energies, whereas panels (a) to (f) show the magnetic field components in inertial RTN system, where the radial component  $R$  is oriented along the Sun–spacecraft line, the magnetic field azimuthal angle  $\phi_B$ , the normalized e-PADs, the solar wind proton number density  $N_p$ , the bulk speed  $V_p$ , and the proton temperature  $T_p$ , respectively. In the left figure, panel (g) shows the omnidirectional ion intensities measured by EPD/EPT, whereas panels (h) to (j) display the ion intensities measured by the “Asun” and “Sun” telescopes of EPD/EPT along with their intensity ratios, respectively. The energy range in panels (h)–(i) is from 0.05 MeV to about 6 MeV, as indicated by the blue to red colors, and it is the same to the y-axis of panel (j), whereas the color bar in panel (j) shows the ratios. The unit of the differential intensities is  $\text{cm}^{-2} \text{sr}^{-1} \text{s}^{-1} \text{MeV}^{-1}$ . Similarly, panels (g)–(j) in the right figure present the energetic ions observed by SEPT onboard STEREO A. The solid vertical lines in both figures mark the ion enhancements investigated in this work, and the shaded regions indicate an SFR observed by both spacecraft.

toward the north and south ecliptic poles with small inclination, respectively (J. Rodríguez-Pacheco et al. 2020).

### 3. Observations

#### 3.1. Overview

This section provides an overview of the targeted event observed by Solar Orbiter and STEREO A. As shown in Figure 1, Solar Orbiter was situated at  $\sim 0.72$  au from the Sun with a Carrington longitude of about  $242^\circ$  and latitude of about  $-3^\circ$ , while STEREO A was located at  $\sim 0.97$  au with a Carrington longitude of about  $223^\circ$  and latitude of about  $-5^\circ$ , providing a perfect opportunity for comparing observations nearly along the same nominal Parker spiral.

In Figure 2, the left figure presents Solar Orbiter observations, with the corresponding STEREO A observations in the same format on the right. Starting from the left figure, the top panel shows the energetic ion intensities of the widespread SEP event at several selected energies, whereas the bottom panels display the background solar wind and the directional energetic ion distributions around the identified ion enhancement of interest as marked by the two solid vertical lines, which occurs in the rising phase of the widespread SEP event. In the bottom panels, the magnetic field components in RTN coordinates are exhibited in panel (a), and the azimuthal angle  $\phi_B$  is illustrated in panel (b). Panel (c) displays the normalized e-PADs, followed by panels (d) to (f) showing the solar wind proton number density  $N_p$ , bulk speed  $V_p$ , and proton temperature  $T_p$ , respectively. Panel (g) provides insights into the omnidirectional ion intensities

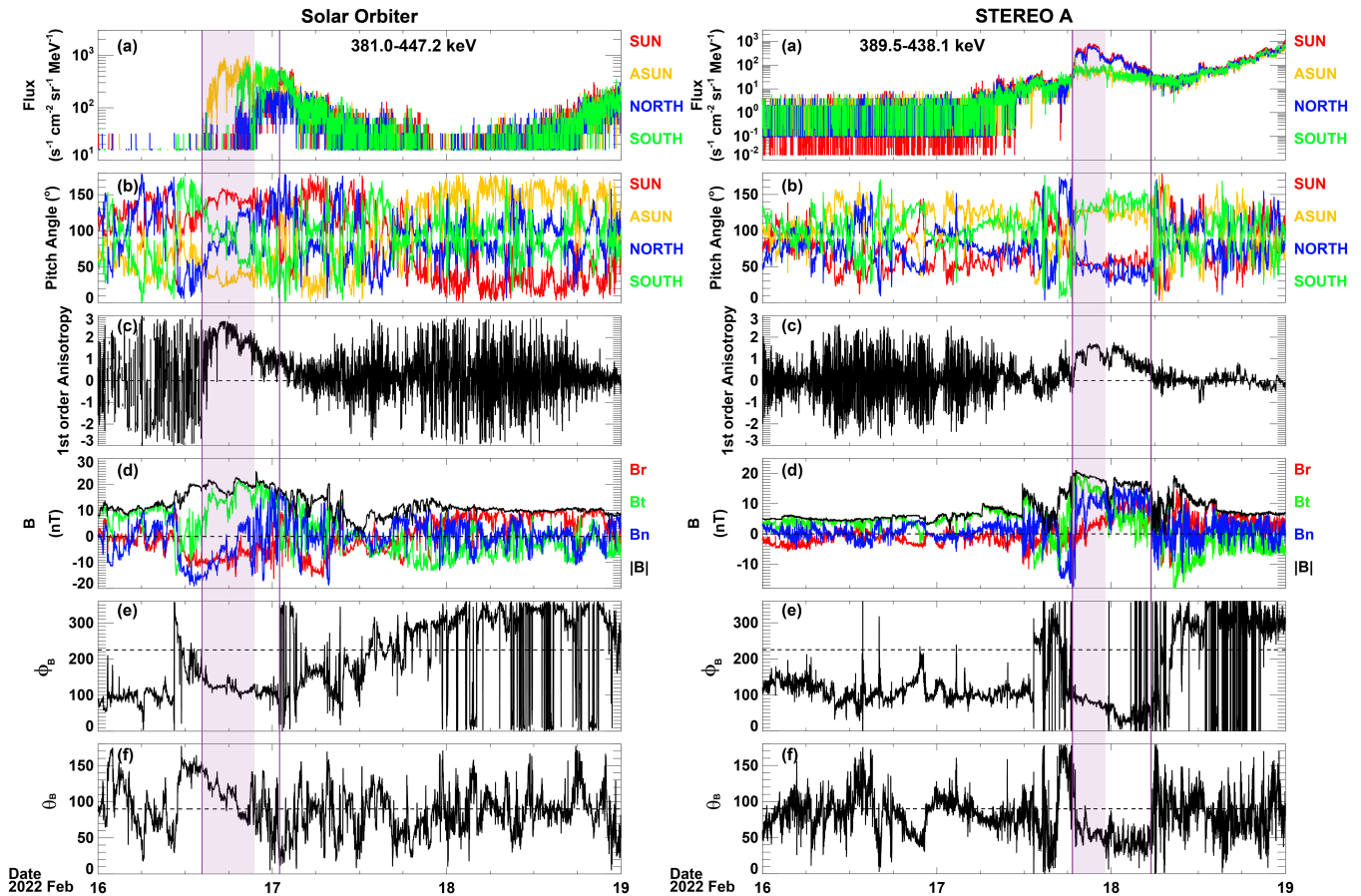


**Figure 3.** Energetic ions and magnetic field topology observed by Solar Orbiter (left figure) and STEREO A (right figure). The top panels show ions observed by EPD/EPT (381.0–447.2 keV) and SEPT (389.5–438.1 keV) in their four viewing directions, respectively. Panels (b) plot the pitch angles of the center axes of the four directions of the EPD/EPT and SEPT telescopes, respectively. Panels (c) show the first-order anisotropy. Panels (d), (e), and (f) present the magnetic field components in RTN coordinates, the azimuthal angle  $\phi_B$ , and the elevation angle  $\theta_B$  from both spacecraft. The vertical lines and shaded regions have the same meanings as Figure 2.

measured by EPD/EPT onboard Solar Orbiter, and panels (h) and (i) present the ion intensities measured by the “Asun” and “Sun” telescopes of EPD/EPT, with panel (j) indicating the directional intensity ratios between the two viewing directions (“Asun/Sun”). Similarly, the right figure presents the STEREO A observations, with panels (g) to (j) representing the corresponding measurements from SEPT onboard STEREO A. The energetic ion enhancement examined in this study is marked by the solid vertical lines in both figures, whereas a small flux rope (SFR) is marked by the shaded region. The ion enhancement period at STEREO A was selected between the two density pileup regions as shown in panel (d), and it was accompanied by a very large and long-lasting anisotropy as shown in the right Figure 3(c). The ion enhancement period at Solar Orbiter was predominantly selected around its peak that was also notable for the very large and long-lasting anisotropy, as shown in the left panel of Figure 3(c). Additionally, the ion enhancements detected by STEREO A and Solar Orbiter were separated by approximately 28.3 hr.

A comparison of both observations implies that the ion enhancements observed in both locations occurred under similar background solar wind conditions. As shown in panel (d) of STEREO A observations, there are two outstanding density enhancements. The leading one is an SIR that was formed by the fast solar wind overtaking the slow wind, as indicated in panels (e) and (f), and a shock at its leading edge is characterized by jumps of magnetic field strength and proton

speed, density, and temperature, as shown in panels (a) and (d)–(f). The trailing one is a heliospheric plasma sheet (HPS) that is adjacent to a heliospheric current sheet (HCS), which is distinguished by the major reversals of  $\phi_B$  in panel (b) and e-PADs in panel (c). In comparison with STEREO A observations, Solar Orbiter also recorded two density enhancements, with the leading one to be an SIR and the trailing one to be a HPS that embeds multiple current sheet crossings, which is frequently observed in the inner heliosphere (A. Szabo et al. 2020; J. Huang et al. 2023), as indicated by the variations of  $\phi_B$  and e-PADs. However, the leading edge of the Solar Orbiter SIR does not show a clear shock feature in comparison with the STEREO A measurements, implying that the SIR-driven shock is not yet well developed at Solar Orbiter’s location. We note that the SIR and HCS/HPS are also separated by about one day between the two observers. In general, the SIR and HCS/HPS structures are indicators of corotating background solar wind. Together with the fact that the two spacecraft are almost aligned along the same nominal Parker spiral, we can infer that the solar wind between the two highly structured density enhancements should be relatively stable as they corotate from Solar Orbiter to STEREO A. In the selected region between the SIR and HCS/HPS in both observations, the leading part is an SFR featured by magnetic field rotation (panels (a)–(b)), low proton temperature (panel (f)), and low plasma beta (not shown), but the unidirectional e-PADs indicate that its

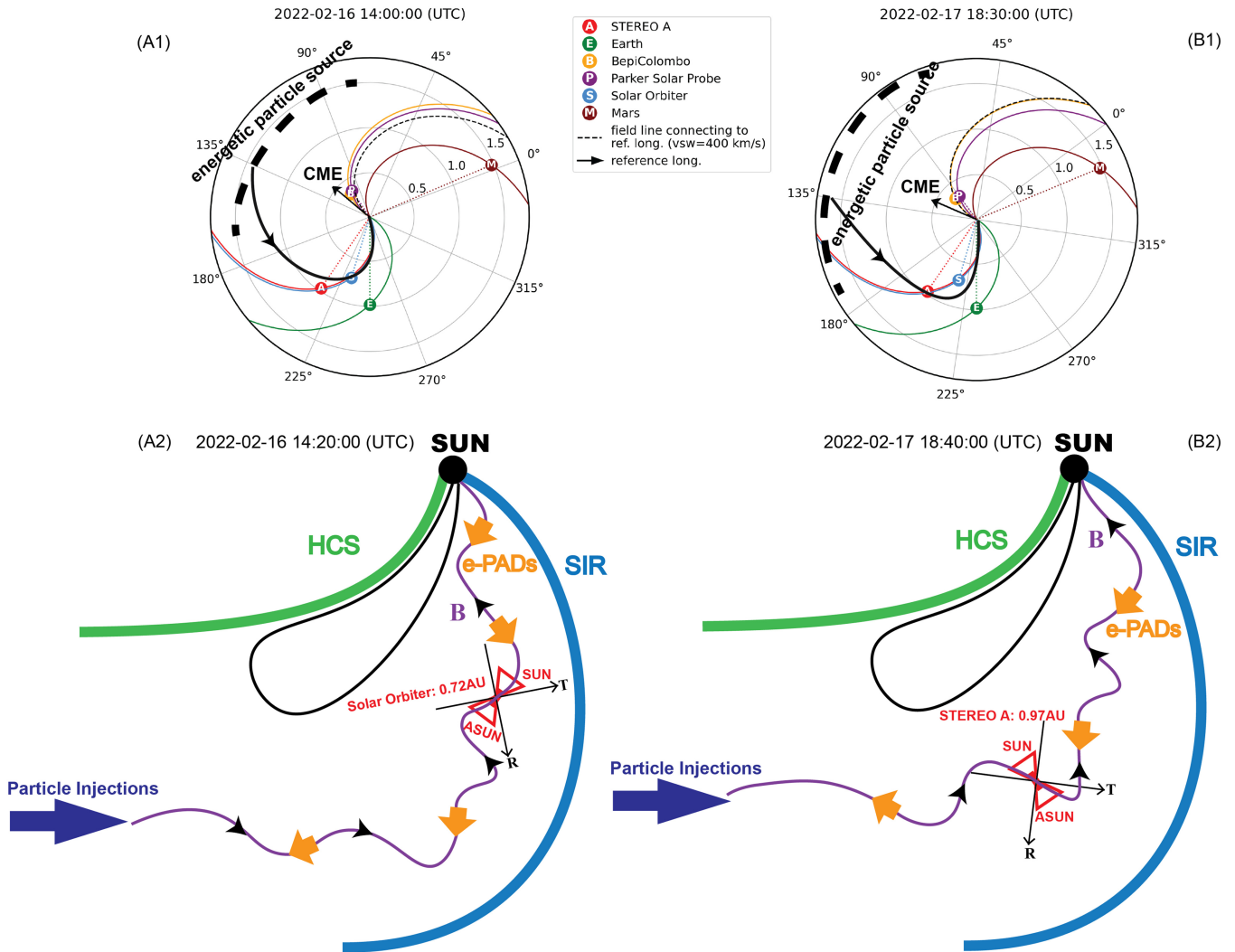


**Figure 4.** A sketch to describe Solar Orbiter (A1–A2) and STEREO A (B1–B2) observations; details are given in the main text. Figures (A1) and (B1) show the positions of Solar Orbiter and STEREO A, as shown in Figure 1. The CME propagation direction is marked by the black arrow, and the possible energetic particle source associated with the CME-driven shock is indicated by the bold dashed line. Figures (A2) and (B2) indicate the solar wind structures and particle features when Solar Orbiter and STEREO A encounter the focused anisotropy event at different locations, respectively. In the figures, an open SFR (purple line) and a following closed loop (black line) are embedded between the SIR (blue line) and the HCS (green line). Moreover, the antisunward-flowing suprathermal electrons (gold arrows), magnetic field directions (black arrows), energetic particle injections (blue arrow), and the instrument viewing directions (red sketch) are displayed in the open SFR.

magnetic field lines are open, whereas the trailing part shows bidirectional e-PADs, implying a closed magnetic field topology, as shown in Figure 4 that will be discussed in Section 4.

Despite the similarities in the background solar wind, the energetic ions show opposite directional distributions between Solar Orbiter and STEREO A. Panels (g) of Figure 2 illustrate omnidirectional ion intensities from about 0.1 to 6.0 MeV, which are similar between the two observers. A closer look at the ion distributions, as shown in panels (h) and (i), indicates different ion intensities in the sunward and antisunward directions within the selected regions. The left figure shows that the ions recorded by the “Asun” telescope are more intense than that in the “Sun” direction by Solar Orbiter. However, STEREO A observed a reversed feature, as shown in the right figure, with the ion intensities measured by the “Asun” telescope being significantly lower than those observed from the “Sun” one. This feature is more visible in panels (j), which present the directional intensity ratios between the two telescopes (“Asun/Sun”). We can see the directional “Asun/

Sun” ratios are nearly opposite in the selected regions, but they are nearly isotropic in the leading and trailing regions, although the differences in the leading regions are affected by low data statistics. The opposite directional distributions of energetic ions in a relatively stable solar wind background along the Parker spiral could be caused by the rotated orientation of the STEREO instruments or variations in the local magnetic field vectors; thus, a necessary step is to check the pitch angle distributions because comparing the viewing directions of the instruments alone could be misleading.

### 3.2. Pitch Angle Distributions

In this section, we investigate the pitch angle distributions of energetic ions to understand their directional differences between Solar Orbiter and STEREO A. Figure 3 shows the energetic ion distributions along with the magnetic field observations from Solar Orbiter (left figure) and STEREO A (right figure) in the same format. Panels (a) present the ion intensities at around 412 keV detected by the four telescopes of

EPD/EPT and IMPACT/SEPT, whereas panels (b) exhibit the corresponding pitch angles of the four telescopes. Panels (c) illustrate the first-order anisotropy that is calculated with the following equation (N. Dresing et al. 2014; M. Brüdern et al. 2018):

$$A_1 = 3 \frac{\int_{-1}^{+1} I(\mu) \cdot \mu \cdot d\mu}{\int_{-1}^{+1} I(\mu) \cdot d\mu}, \quad (1)$$

where  $I(\mu)$  represents the pitch-angle-dependent intensity measured in a given viewing direction and  $\mu$  is the average pitch angle cosine for that direction. Moreover, panels (d), (e), and (f) display the magnetic field components as well as their  $\phi_B$  and  $\theta_B$  angles in RTN coordinates observed by both spacecraft.

This figure reveals several outstanding characteristics of the ion enhancement marked by the shaded region:

1. **Magnetic Field Topology.** As shown in panels (d)–(f) of Figure 3, Solar Orbiter observes predominantly a negative radial magnetic field  $B_r$  and a near-Parker-spiral  $\phi_B$  angle ( $\sim 135^\circ$ ), but STEREO A measures mainly a positive  $B_r$  with  $\phi_B$  varying below  $90^\circ$ . This suggests that the magnetic field topology and/or connectivity is different between the two observers.
2. **Energetic Ion Intensities.** For Solar Orbiter, the intensity measured by the “Asun” telescope at pitch angles approximately around  $30^\circ$  exceeds that by the “Sun” telescope near  $150^\circ$ , as shown in panels (a) and (b). In addition, energetic ions detected by the “Asun” telescope start to rise about 6.32 hr earlier than those detected by the “Sun” telescope (panel (a)). In contrast, STEREO A observes higher ion intensity from the “Sun” telescope (pitch angles around  $50^\circ$ ) than that from the “Asun” sensor (pitch angles around  $130^\circ$ ). Furthermore, there is no time delay in ion intensity enhancements between the two directions, as suggested by panel (a), and the ion intensities inside the SFR are much higher than those in the trailing part. The earliest ion enhancement starts around 14:20 UT on February 16 for Solar Orbiter, whereas it appears around 18:40 UT on February 17 for STEREO A, indicating a time difference of about 28.3 hr.
3. **First-order Anisotropy.** In both figures, panels (c) display notable and long-lasting first-order anisotropy  $A_1$  in the marked region, whereas  $A_1$  is highly fluctuating in the leading and trailing regions, which is caused by poor statistics in the intensity data and should not be interpreted as a real anisotropy. In general, if the energetic ions are mainly from the Sun and predominately propagate along the magnetic field line,  $A_1$  should be negative when the average pitch angle cosine ( $\mu$ ) of antisunward streaming particles is negative and vice versa. However, Solar Orbiter observes long-lasting positive  $A_1$  under the observed magnetic field topology, and the largest  $A_1$  is 2.76, which is close to the theoretically extreme value of 3. Such a large, sustained anisotropy is unexpected and could offer insights into the underlying behavior of energetic ions of solar origin in the heliosphere, as discussed below. Moreover, STEREO A observes a long-lasting positive  $A_1$  with a smaller value of 1.76, which is comparable in the SFR and its trailing region.

## 4. Discussion

Based on the above detailed analysis of the observations, there are two outstanding features of this event: one feature is the directional differences of energetic ion distributions between Solar Orbiter and STEREO A, and the other is the very large and long-lasting first-order anisotropy in this event. In this section, we discuss the possible mechanisms that might be responsible for these features.

Directional differences of energetic ion distributions between Solar Orbiter and STEREO A could be caused by the twisted and deflected magnetic field topology of the SFR. As introduced in Section 2, EPD/EPT is pointing sunward and antisunward along the nominal Parker spiral. Moreover,  $\phi_B$  is around  $120^\circ$  at Solar Orbiter, indicating the energetic ions entering the two sensors mainly along the magnetic field directions, which is evident from their pitch angle distributions and magnetic field topology (see panels (b) and (d)–(f) in the left Figure 3). Furthermore, after the solar conjunction of STEREO A, SEPT changed its nominal pointing directions during this event, which adds difficulties in understanding the directional information correctly. Fortunately,  $\phi_B$  varies between  $\sim 25^\circ$  and  $\sim 90^\circ$  and  $\theta_B$  lies at  $\sim 60^\circ$ , suggesting that the magnetic field lines generally align with the “Sun/North–Asun/South” look directions of SEPT, so the directional information could be inferred relatively easily. As shown in Figures 4(A2)–(B2), the “Sun” and “Asun” look directions of EPT and SEPT are represented by the red triangles at the locations of Solar Orbiter and STEREO A, and the observed magnetic field directions are marked by the purple solid lines with black arrows. Solar Orbiter and STEREO A are roughly aligned along the same nominal Parker spiral, as indicated in Figures 4(A1)–(B1), but the actual magnetic field lines between them could be globally deflected from the Parker spiral, as indicated by the black solid lines, and also twisted to be out of the ecliptic plane due to the passage of the SFR. As a result, the “Sun” and “Asun” telescopes of SEPT should measure the ions observed by the “Asun” and “Sun” telescopes of EPT, respectively. Therefore, the directional differences of energetic ion distributions between Solar Orbiter and STEREO A should be caused by the deflected and also twisted magnetic field topology.

The long-lasting anisotropy implies that the sunward streaming energetic ions could be injected from a particle source located beyond STEREO A. As introduced in Section 3.2, if the Sun is the particle source, the first-order anisotropy  $A_1$  should be negative when the average pitch angle cosine ( $\mu$ ) of antisunward streaming particles is negative and vice versa. Considering the magnetic field topology at both Solar Orbiter and STEREO A, the anisotropies of energetic ions at both observers are anticipated to be negative; hence, the positive  $A_1$  values mean that the energetic ions are predominantly streaming toward the Sun, which is also supported by their pitch angle distributions, as shown in panels (a)–(b) of Figure 3. Sunward streaming particles have been studied previously, with the most common explanation being related to the closed loops of magnetic clouds channeling particles injected from the far leg that is still rooted at the Sun (e.g., R. Gómez-Herrero et al. 2017; N. Dresing et al. 2018, and references therein), although particles could also be injected from beyond an observer’s heliocentric distance by a CME-driven shock (R. Leske et al. 2015) or reflected by magnetic mirrors in magnetic field structure (L. C. Tan et al. 2012; G. Li et al. 2020). For this event, as shown in Figure 2(c),

the SFR shows single directional e-PADs, indicating an open magnetic field topology of the structure. Combining the magnetic field direction and the e-PADs, we deduce that the suprathermal electrons are flowing antisunward along the open magnetic field lines, so the “correct” electron flowing direction indicates that the SFR should only have one leg connected to the Sun, as suggested by the purple line in Figures 4(A2)–(B2). The open SFR structures are intriguing but not rare. Studies indicate that they can form in evolving stream structures or slow CMEs (B. J. Lynch et al. 2016, 2021) through magnetic reconnection (H. Tian et al. 2010; B. Lavraud et al. 2014; J. Huang et al. 2018). As a result, the injection from a far leg of closed loops as an explanation for the sunward streaming energetic ions does not apply for this event. Instead, the energetic ions must come from a source beyond the spacecraft locations. However, we are unable to determine the velocity dispersion to calculate the path length between the particle source and the observer, due to the mixing of the injected ions with ions from both the leading SIR and the gradual SEP event, making it difficult to pinpoint the onset times of the sunward streaming ions.

The very large anisotropy between STEREO A and Solar Orbiter gives insights into the transport of energetic ions. At STEREO A, the energetic ion enhancements are mainly observed at pitch angles of  $\sim 50^\circ$  (“Sun” and “North”) and  $\sim 130^\circ$  (“Asun” and “South”) with relatively stable pitch angle distributions. Furthermore, the average intensities during this period are about  $251.2 \text{ (cm}^{-2} \text{ sr}^{-1} \text{ s}^{-1} \text{ MeV}^{-1})$  in the “Sun” and “North” look directions and  $38.6 \text{ (cm}^{-2} \text{ sr}^{-1} \text{ s}^{-1} \text{ MeV}^{-1})$  in the “Asun” and “South” look directions, suggesting a large intensity difference of  $\sim 6.5$  times. Therefore, the very large and long-lasting anisotropy is expected. Meanwhile, the notable directional intensity difference and the ions observed from the antisunward direction further imply that, as shown in Figures 4(A2)–(B2), the magnetic field lines are probably well connected to the inferred source of these energetic ions, which could be associated with the large-scale shock driven by the farside CME event on 2022 February 15. We note that perpendicular diffusion of energetic ions is unlikely in this event, since this process should lead to isotropic pitch angle distributions, and it would not be able to result in the earlier onset of “Asun” ions at Solar Orbiter, as discussed in the following lines.

Solar Orbiter observes an interval of extreme anisotropy  $A_1$  where the energetic ions nearly solely come from the “Asun” direction, implying that the spacecraft is observing the very early phase of ion injections onto the magnetic field lines that are newly connected to the particle source. We note that the average intensities during the focused period at Solar Orbiter are about  $198.6 \text{ (cm}^{-2} \text{ sr}^{-1} \text{ s}^{-1} \text{ MeV}^{-1})$  in the “Asun” and  $131.5 \text{ (cm}^{-2} \text{ sr}^{-1} \text{ s}^{-1} \text{ MeV}^{-1})$  in the “South” look directions and  $71.9 \text{ (cm}^{-2} \text{ sr}^{-1} \text{ s}^{-1} \text{ MeV}^{-1})$  in the “Sun” and  $60.8 \text{ (cm}^{-2} \text{ sr}^{-1} \text{ s}^{-1} \text{ MeV}^{-1})$  in the “North” look directions, i.e., the directional intensity difference between “Asun” and “Sun” is about 2.76 times. Although the directional intensity difference is smaller at Solar Orbiter compared to STEREO A, the maximum  $A_1$  is significantly larger at Solar Orbiter (2.76) than at STEREO A (1.76), as shown in Figure 3(c). We find that the extreme anisotropy appears in the leading part of the targeted region, i.e., the opened SFR, and it approaches the maximum theoretical limit of first-order anisotropy (3.0). The unusually large anisotropy is caused by the high intensity in the “Asun” look direction but very low intensities in the

“Sun,” “South,” and “North” directions for about 6.5 hr. Assuming the sunward streaming ions could be mirrored back by the Sun, we would expect to see a 6.75 hr time delay based on the spacecraft position (0.72 au) and the energetic ions with an energy of about 412 keV. Considering that ions could be mirrored back at several solar radii above the Sun, the expected time delay could be smaller. Therefore, the expected time delay matches well with the observed time delay, suggesting that the antisunward streaming ions detected later by the “Sun” telescope could be the mirrored-back ions from the “Asun” look direction. Consequently, the observations may imply that the magnetic field lines at Solar Orbiter are newly connected to the particle source, and Solar Orbiter is observing the very early phase of the energetic ion injections. However, when STEREO A encounters this enhancement about one day later, the ions have already filled the magnetic field lines; hence, STEREO A observes ions from all four directions.

Lastly, the observed time difference of the focused region between the two spacecraft implies that the magnetic field topology is globally deflected from the nominal Parker spiral. Based on the radial and longitudinal separations of the two spacecraft as introduced in Section 3.1 and the solar wind speed of about  $380 \text{ km s}^{-1}$  in the focused region, the expected time delay of a stable corotating solar wind structure between them should be around 3.4 hr, estimated with the method presented in A. Opitz et al. (2009). However, Solar Orbiter observed this event about 28.3 hr earlier than STEREO A. We suggest that this discrepancy could be well explained by the magnetic field lines being distorted away from the nominal Parker spiral by the drag of the farside CME or the chasing of high-speed streams following the HCS/HPS, as indicated by the solid black lines in Figures 4(A1)–(A2). This is reasonable because SIR and HCS/HPS structures are very similar in both observations, and these large-scale structures are also separated by about one day. These large-scale structures should be an indicator of the corotating background solar wind; hence, the focused regions between them are expected to be at least quasi-stable structures. In addition, there is no ion enhancement simultaneously appearing at both spacecraft (before February 17 at STEREO A and around February 18 at Solar Orbiter). Thus, the long time delay is highly likely to have been caused by the deflected magnetic field topology, as indicated in the sketch.

## 5. Summary


In this work, we report an energetic ion enhancement during the rising phase of the widespread SEP event on 2022 February 15, with Parker spiral-aligned observations by STEREO A and Solar Orbiter. We find two remarkable features of this event: the directional differences of energetic ion distributions between the two spacecraft, and the very large and long-lasting first-order anisotropy during this event. Based on our detailed analysis, we suggest that the magnetic field deflection and the roll of the STEREO A spacecraft lead to the opposite directional distributions of energetic ions between their respective sunward and antisunward orientations. However, the very large and long-lasting first-order anisotropy of this event, its most outstanding feature overall, is most easily explained as the result of continuous injections of energetic ions from a source located in the heliosphere beyond STEREO A, with good magnetic connectivity between both observers and the particle source. However, Solar Orbiter observed an









interval of extremely large anisotropy that is dominated exclusively by sunward streaming ions, which implies the very early phase of ion injections onto the newly connected magnetic field lines between Solar Orbiter and the particle source, likely making it the first reported event of this kind, based on our knowledge. In addition, we show that magnetic connectivity and mirroring effect can work to modify the energetic ion distributions. Our work highlights the value of investigating anisotropy to reveal the source, injection, and transport of energetic ions in future studies.

### Acknowledgments

We acknowledge the use of the STEREO data provided by the STEREO Science Center ([https://stereo-ssc.nascom.nasa.gov/ins\\_data.shtml](https://stereo-ssc.nascom.nasa.gov/ins_data.shtml)) and the Solar Orbiter data from the Solar Orbiter Archive (<https://soar.esac.esa.int/soar/>). W.W. W. and C.O.L. acknowledge support by NASA grants 80NSSC21K1325 and 80NSSC21K0119. N.D. and I.C.J. acknowledge funding by the European Union's Horizon 2020 research and innovation program under grant agreement No. 101004159 (SERPENTINE) and No. 101134999 (SOLER), as well as by the Research Council of Finland (SHOCKSEE; grant No. 346902). L.K.J. thanks the support of NASA's STEREO mission and HGI grant 80NSSC23K0447. B.Z. acknowledges the NASA ECIP grant 80NSSC23K1057 and NSF grant AGS-2301382. J.H. thanks the support of NASA grant 80NSSC23K0737. E.P. acknowledges support from NASA's LWS (grant No. 80NSSC19K0067) and LWS-SC (grant No. 80NSSC22K0893) programs. B.J.L. acknowledges support from NSF AGS-2147399, NASA HGI 80NSSC21K0731, and XRP 80NSSC22K0674. Solar Orbiter is a space mission run as an international collaboration between ESA and NASA and operated by ESA. Solar Orbiter SWA data were derived from scientific sensors that were designed and created and are operated under funding provided by numerous contracts from UKSA, STFC, the Italian Space Agency, CNES, the French National Centre for Scientific Research, the Czech contribution to the ESA PRODEX program, and NASA. SO SWA work at the UCL/Mullard Space Science Laboratory is currently funded by STFC (grant Nos. ST/W001004/1 and ST/X/002152/1).

### ORCID iDs

Wenwen Wei  <https://orcid.org/0000-0001-8495-9179>  
 Christina O. Lee  <https://orcid.org/0000-0002-1604-3326>  
 N. Dresing  <https://orcid.org/0000-0003-3903-4649>  
 L. Y. Khoo  <https://orcid.org/0000-0003-0412-1064>  
 L. K. Jian  <https://orcid.org/0000-0002-6849-5527>  
 J. G. Luhmann  <https://orcid.org/0000-0003-0626-9353>  
 C. M. S. Cohen  <https://orcid.org/0000-0002-0978-8127>  
 F. Fraschetti  <https://orcid.org/0000-0002-5456-4771>

B. Zhuang  <https://orcid.org/0000-0002-5996-0693>  
 J. Huang  <https://orcid.org/0000-0002-9954-4707>  
 C. J. Owen  <https://orcid.org/0000-0002-5982-4667>  
 G. Nicolaou  <https://orcid.org/0000-0003-3623-4928>  
 L. Rodríguez-García  <https://orcid.org/0000-0003-2361-5510>  
 E. Palmerio  <https://orcid.org/0000-0001-6590-3479>  
 I. C. Jebaraj  <https://orcid.org/0000-0002-0606-7172>  
 B. J. Lynch  <https://orcid.org/0000-0001-6886-855X>  
 F. Carcaboso  <https://orcid.org/0000-0003-1758-6194>

### References

- Acuña, M. H., Curtis, D., Scheifele, J. L., et al. 2008, *SSRv*, 136, 203  
 Bieber, J. W., Dröge, W., Evenson, P. A., et al. 2002, *ApJ*, 567, 622  
 Brüderm, M., Dresing, N., Heber, B., et al. 2018, *CEAB*, 42, 2  
 Cohen, C. M. S., Leske, R. A., St. Cyr, O. C., & Mason, G. M. 2024, *ApJL*, 966, L19  
 Dresing, N., Gómez-Herrero, R., Heber, B., et al. 2014, *A&A*, 567, A27  
 Dresing, N., Gómez-Herrero, R., Heber, B., et al. 2016, *A&A*, 586, A55  
 Dresing, N., Gómez-Herrero, R., Heber, B., et al. 2018, *A&A*, 613, A21  
 Dresing, N., Rodríguez-García, L., Jebaraj, I., et al. 2023, *A&A*, 674, A105  
 Dwyer, J. R., Mason, G. M., Mazur, J. E., et al. 1997, *ApJL*, 490, L115  
 Galvin, A. B., Kistler, L. M., Popecki, M. A., et al. 2008, *SSRv*, 136, 437  
 Giacalone, J., Cohen, C. M. S., McComas, D. J., et al. 2023, *ApJ*, 958, 144  
 Gieseler, J., Dresing, N., Palmroos, C., et al. 2023, *FrASS*, 9, 1058810  
 Gómez-Herrero, R., Dresing, N., Klassen, A., et al. 2017, *ApJ*, 840, 85  
 Horbury, T. S., O'Brien, H., Carrasco Blazquez, I., et al. 2020, *A&A*, 642, A9  
 Huang, J., Kasper, J. C., Larson, D. E., et al. 2023, *ApJS*, 265, 47  
 Huang, J., Liu, Y. C.-M., Peng, J., et al. 2018, *JGRA*, 123, 7167  
 Jebaraj, I. C., Dresing, N., Krasnoselskikh, V., et al. 2023b, *A&A*, 680, L7  
 Jebaraj, I. C., Kouloumvakos, A., Dresing, N., et al. 2023a, *A&A*, 675, A27  
 Kaiser, M. L., Kucera, T. A., Davila, J. M., et al. 2008, *SSRv*, 136, 5  
 Khoo, L. Y., Sánchez-Cano, B., Lee, C. O., et al. 2024, *ApJ*, 963, 107  
 Lario, D., Wijsen, N., Kwon, R. Y., et al. 2022, *ApJ*, 934, 55  
 Lavraud, B., Ruffenach, A., Rouillard, A. P., et al. 2014, *JGRA*, 119, 26  
 Leske, R., Cummings, A., Cohen, C., et al. 2015, *ICRC (The Hague)*, 34, 72  
 Li, G., Wu, X., Zhao, L., & Yao, S. 2020, *ApJL*, 905, L1  
 Luhmann, J. G., Curtis, D. W., Schroeder, P., et al. 2008, *SSRv*, 136, 117  
 Lynch, B. J., Masson, S., Li, Y., et al. 2016, *JGRA*, 121, 10677  
 Lynch, B. J., Palmerio, E., DeVore, C. R., et al. 2021, *ApJ*, 914, 39  
 Mierla, M., Zhukov, A. N., Berghmans, D., et al. 2022, *A&A*, 662, L5  
 Müller, D., St. Cyr, O. C., Zouganelis, I., et al. 2020, *A&A*, 642, A1  
 Müller-Mellin, R., Böttcher, S., Falenski, J., et al. 2008, *SSRv*, 136, 363  
 Opitz, A., Karrer, R., Wurz, P., et al. 2009, *SoPh*, 256, 365  
 Owen, C. J., Bruno, R., Livi, S., et al. 2020, *A&A*, 642, A16  
 Palmerio, E., Carcaboso, F., Khoo, L. Y., et al. 2024, *ApJ*, 963, 108  
 Rodríguez-Pacheco, J., Wimmer-Schweingruber, R. F., Mason, G. M., et al. 2020, *A&A*, 642, A7  
 Sauvaud, J. A., Larson, D., Aoustin, C., et al. 2008, *SSRv*, 136, 227  
 Strauss, R. D. T., Dresing, N., & Engelbrecht, N. E. 2017, *ApJ*, 837, 43  
 Szabo, A., Larson, D., Whittlesey, P., et al. 2020, *ApJS*, 246, 47  
 Tan, L. C., Malandraki, O. E., Reames, D. V., et al. 2012, *ApJ*, 750, 146  
 Tan, L. C., Reames, D. V., & Ng, C. K. 2007, *ApJ*, 661, 1297  
 Tian, H., Yao, S., Zong, Q., He, J., & Qi, Y. 2010, *ApJ*, 720, 454  
 Wang, Y., Qin, G., & Zhang, M. 2012, *ApJ*, 752, 37  
 Wei, W., Shen, F., Yang, Z., et al. 2019, *JASTP*, 182, 155  
 Wei, W., Zhuang, B., Huang, J., et al. 2022, *JGRA*, 127, e2022JA030652  
 Zhuang, B., Lugaz, N., & Lario, D. 2022, *ApJ*, 925, 96